Skyrmions in a ferromagnetic Bose–Einstein condensate

Usama Al Khawaja & Henk Stoof

Institute for Theoretical Physics, University of Utrecht, Princetonplein 5, 3584 CC Utrecht, The Netherlands

Multi-component Bose–Einstein condensates[1–3] provide opportunities to explore experimentally the wealth of physics associated with the spin degrees of freedom[4–7]. The ground-state properties[8–11] and line-like vortex excitations[8,12,13] of these quantum systems have been studied theoretically. In principle, nontrivial spin textures consisting of point-like topological excitations, or skyrmions[14,15], could exist in a multi-component Bose–Einstein condensate, owing to the superfluid nature of the gas. Although skyrmion excitations are already known in the context of nuclear physics and the quantum-Hall effect, creating these excitations in an atomic condensate would offer an opportunity to study their physical behaviour in much greater detail, while also enabling an *ab initio* comparison between theory and experiment. Here we investigate theoretically the stability of skyrmions in a fictitious spin-1/2 condensate of ^{87}Rb atoms. We find that skyrmions can exist in such a gas only as a metastable state, but with a lifetime comparable to (or even longer than) the typical lifetime of the condensate itself.

An essential feature of a spinor Bose–Einstein condensate is that two or more hyperfine states of the atoms in the condensate have almost the same energy. As a result, this spin degree of freedom becomes a relevant dynamical variable, which gives rise to new excitations that are not present in the usual single-component Bose–Einstein condensates, where the spins are effectively frozen. One of these excitations is the skyrmion, which is a topological nontrivial spin texture. Roughly speaking, the skyrmion is a point-like object that can be created out of the ground state, in which all the spins are aligned, by reversing the average spin in a finite region of space. Although topological considerations indeed allow for these excitations, which we note are fundamentally different from the topologically trivial coreless vortices discussed in ref. 8, we need to know whether such a configuration is also energetically stable. However, when solving the appropriate Gross–Pitaevskii equation[8], we find that, in equilibrium, the energy is always minimized by collapsing the skyrmion to zero size. Fortunately, it turns out that for sufficiently small sizes of the skyrmion a nonequilibrium stability mechanism starts to work. A number of atoms in the centre of the skyrmion, which we denote here as the core atoms, will be trapped by an effective three-dimensional potential barrier, that is, a repulsive shell with a finite radius that is induced by the gradients in the spin texture of the skyrmion itself. As the skyrmion shrinks in size, the barrier height of the repulsive shell increases and the radius decreases. This leads to a squeezing of the core atoms and thus to an increase in their energy, which ultimately stabilizes the skyrmion. As mentioned, this is not an equilibrium state of the condensate because the core atoms will tunnel over the barrier and give the skyrmion a finite lifetime. We note that our calculations are for a uniform condensate. However, our results are also valid for trapped gases, as the size of the skyrmion always turns out to be of the order of the correlation length of the condensate, which is typically much smaller than the size of the condensate. Moreover, in order to produce realistic estimates that can be compared with future experiments, we discuss only the case of a spin-1/2 ^{87}Rb condensate, because the spin-1 ^{23}Na condensate that has also been realized experimentally has an antiferromagnetic ground state.

We thus consider a uniform condensate of constant density n and constant spinor $\zeta_z = (1, 0)$, with all spins being oriented in the positive z-direction. This represents the ground state of the gas. For the skyrmion, however, both n and ζ are position-dependent. A convenient way to take the position dependence of $\zeta(\mathbf{r})$ into account is to express the spinor as $\zeta(\mathbf{r}) = \exp\{-i2\boldsymbol{\Omega}(\mathbf{r})\cdot\hat{\mathbf{S}}\}\zeta_z$, where $\hat{\mathbf{S}}$ are the usual angular momentum operators for spin-1/2. The physical meaning of this formula is that the average spin at a position $\mathbf{r}$ is rotated by an angle $2\Omega(\mathbf{r})$ from its initial orientation with $\boldsymbol{\Omega}(\mathbf{r})/\Omega(\mathbf{r})$ the axis of rotation. An explicit form of $\boldsymbol{\Omega}(\mathbf{r})$ now determines a specific texture of the skyrmion. We consider only the most symmetric shape of the skyrmion, because on general grounds this is expected to have the lowest energy. We thus take $\boldsymbol{\Omega}(\mathbf{r}) = \omega(r)\mathbf{r}/r$. The boundary conditions at $r = 0$ and $r \to \infty$ that the function $\omega(r)$ should satisfy are the following. First, at $r \to \infty$ all spins must be oriented as in the ground state, since otherwise it requires an infinite amount of energy to create the skyrmion. This implies $\lim_{r\to\infty}\omega(r) = 0$. Along the z-axis the spins are also not rotated by our ansatz for $\boldsymbol{\Omega}(\mathbf{r})$, so in order to have a nonsingular texture of the spinor with a non-zero winding number, we must require that $\omega(0) = 2\pi$. Finally, to avoid a singular behaviour of $\boldsymbol{\Omega}(\mathbf{r})$ itself, we take only functions $\omega(r)$ with zero slope at the origin. In summary, $\omega(r)$ is therefore a monotonically decreasing function that starts from 2π at the origin and reaches zero when $r \to \infty$. The specific functional form of $\omega(r)$ at intermediate distances between zero and infinity is not crucial for the stability of the skyrmion. Only the above boundary conditions are important for that.

From a quantum mechanical point of view, the condensate is described by a macroscopic wavefunction, or order parameter, $\psi(\mathbf{r}) \equiv \sqrt{n(\mathbf{r})}\zeta(\mathbf{r})$. Furthermore, the grand-canonical energy (energy − number of atoms times chemical potential) of the gas can in the usual mean-field approximation be expressed as a function of $n(\mathbf{r})$ and $\zeta(\mathbf{r})$[8]. In detail, we have:

$$E[n(\mathbf{r}),\zeta(\mathbf{r})] \equiv \int d\mathbf{r}\left[\frac{\hbar^2}{2m}\left(\nabla\sqrt{n(\mathbf{r})}\right)^2 - \mu n(\mathbf{r}) + \frac{\hbar^2}{2m}n(\mathbf{r})|\nabla\zeta(\mathbf{r})|^2 + \frac{1}{2}T^{2B}n^2(\mathbf{r})\right] \quad (1)$$

where m is the mass of the atoms, μ is their chemical potential and $T^{2B} = 4\pi a\hbar^2/m$ is the appropriate coupling constant that represents the strength of the interatomic interactions in terms of the positive scattering length a. It is clear from the above expression that the gradients in the spin texture lead to a contribution to the energy density, which is proportional to $|\nabla\zeta(\mathbf{r})|^2$. Using the above-mentioned form of $\zeta(\mathbf{r})$ and inserting the explicit forms of the spin-1/2 matrices, the square of the spinor gradient can be written explicitly as:

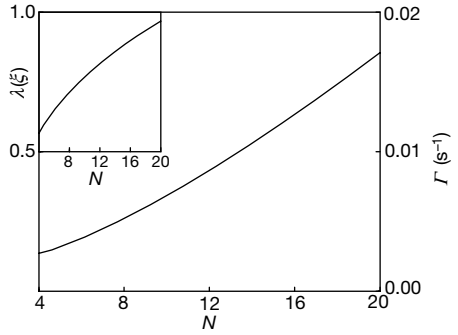

Figure 1 Decay rate Γ and size λ (inset) of the skyrmion as a function of the number of atoms trapped in the core. The two curves are calculated for the parameters of a ^{87}Rb spinor condensate with a density of 10^{13} cm^{-3}. The size is calculated in units of the correlation length ξ, which for these parameters equals 0.85 μm.

$$|\nabla\zeta(\mathbf{r})|^2 = 2\left(\frac{\sin(\omega(r))}{r}\right)^2 + \left(\frac{\mathrm{d}\omega(r)}{\mathrm{d}r}\right)^2 \qquad (2)$$

In principle, both $n(r)$ and $\omega(r)$ can now be calculated exactly by minimizing the energy functional in equation (1) with respect to arbitrary functions $n(r)$ and $\omega(r)$ that satisfy the boundary conditions. However, the resulting nonlinear and coupled equations are quite difficult to solve. Therefore, we use here a variational approach and take for $\omega(r)$ the simple ansatz $\omega(r) = 4\cot^{-1}[(r/\lambda)^2]$, where the variational parameter λ physically corresponds to the size of the skyrmion. This ansatz is chosen here because it automatically incorporates the correct boundary conditions and leads to a minimal skyrmion energy as compared to other ansatzes that we have considered. Having specified $\omega(r)$, we then calculate $n(r)$ exactly by solving numerically the differential equation for $n(r)$ obtained by varying $E[n(\mathbf{r}), \zeta(\mathbf{r})]$ with respect to $n(r)$. Substituting this density profile back into the energy functional, the energy of the skyrmion becomes a function of λ only and the equilibrium properties can be obtained by minimizing this energy with respect to λ.

Inserting our ansatz for $\omega(r)$ in equation (2), $\hbar^2|\nabla\zeta(\mathbf{r})|^2/2m$ takes the shape of an off-centred potential barrier with a maximum of $24.3\hbar^2/2m\lambda^2$ located at 0.68λ. We now distinguish between two cases. The first case occurs when the height of the barrier is lower than the chemical potential μ of the atoms. In this case, atoms can move freely across the barrier and equilibrium is quickly achieved. In the second case, the barrier height is higher than the chemical potential and thus atoms become trapped behind the barrier near the centre of the skyrmion. Equating the barrier height with $\mu = T^{2B}n$ gives therefore the maximum value of $\lambda_{max} \approx 5\xi$ below which trapping takes place. Here ξ is the correlation length given by $\xi = 1/\sqrt{8\pi an}$, and n is the density at $r \gg \lambda$. For $\lambda < \lambda_{max}$ we calculate first the metastable size of the skyrmion by minimizing for a fixed number of core atoms the total energy of the condensate. Next we calculate the tunnelling rate for the core atoms to escape to the outer region (see Methods). The results of these calculations are presented in Fig. 1, where we plot the metastable size of the skyrmion as a function of the number of the core atoms trapped by the texture barrier, together with the corresponding tunnelling rate. As mentioned previously, we use the parameters of ^{87}Rb with a density of $n = 10^{13}\,\mathrm{cm}^{-3}$. We see from Fig. 1 that only a few atoms in the core of the skyrmion are needed to stabilize it and to give it a sufficiently long lifetime. We note that the tunnelling rate is considerably less than the decay rate of the condensate, which is due to two-body collisions[16] and equal to Gn with a measured value of[1] $G \approx 2.2 \times 10^{-14}\,\mathrm{cm}^{-3}\,\mathrm{s}^{-1}$. Also, the lifetime becomes even larger for slightly smaller values of n.

Next, we address some of the interesting properties of the skyrmion, which are its texture and its dynamics. The texture can best be presented in terms of the three average spin components $\langle S_z\rangle(\mathbf{r}) \equiv \zeta^+(\mathbf{r})\hat{S}_z\zeta(\mathbf{r})$, $\langle S_y\rangle(\mathbf{r})$, and $\langle S_x\rangle(\mathbf{r})$ in the three cartesian planes. These are shown in Fig. 2. The most interesting dynamical property of the skyrmion comes from the fact that if all spins of the texture are rotated around the z axis by a constant angle θ, that is, $\zeta(\mathbf{r}) \rightarrow \exp(-i\theta\hat{S}_z)\zeta(\mathbf{r})$, the resulting skyrmion will have the same energy. As a result, the angle θ undergoes phase diffusion. It also leads to a Josephson-like coupling between two skyrmions, which will have important consequences for the physics of the skyrmion lattice[17] that, as in an Abrikosov vortex lattice, will form at sufficiently low temperatures. Another dynamical property is the centre-of-mass motion of the skyrmion, which can be shown to be identical to that of a massive particle. As a result the skyrmion will be accelerated towards the edge of the condensate in a trapped situation.

Although skyrmion–antiskyrmion pairs can be created by the Kibble mechanism in a temperature quench or by sufficiently shaking up the condensate, a more controlled way of creating a skyrmion can be achieved by using a magnetic field configuration in which the fictitious magnetic field is always pointing radially outward and its magnitude increases monotonically from zero at the origin to a maximum value for large distances from the origin. Applying this field configuration for such a long time that the spins at large distances have precessed exactly twice around the local magnetic field, creates a single skyrmion. Of course, for a real magnetic field the above configuration requires the use of magnetic monopoles, but for a fictitious magnetic field it can be achieved by appropriately tailoring the detuning, the polarization, and the intensity of two pulsed Raman lasers. The required spatial dependence of the detuning can be created experimentally by separating

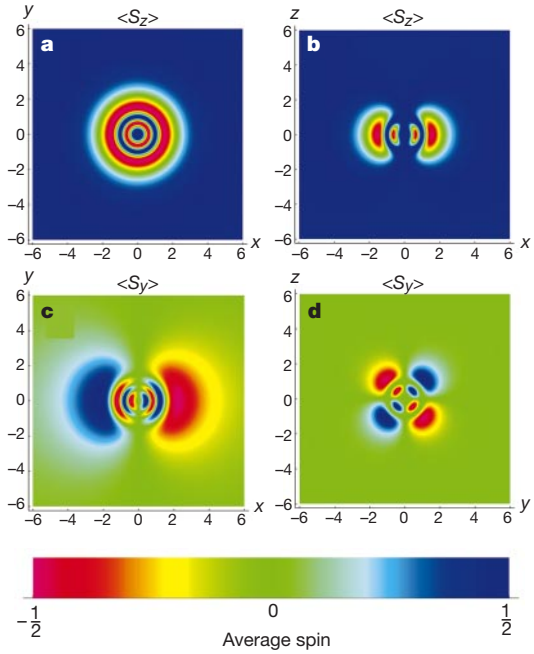

Figure 2 The average spin texture of the skyrmion. Shown are the components $\langle S_z\rangle(\mathbf{r}) = \zeta^+(\mathbf{r})\hat{S}_z\zeta(\mathbf{r})$ and $\langle S_y\rangle(\mathbf{r})$ in the three cartesian planes. A value of $\lambda = \xi$, which corresponds to 20 core atoms, was chosen to compute these quantities. The distances are in units of the coherence length ξ. The $\langle S_x\rangle(\mathbf{r})$ component can be obtained from the $\langle S_y\rangle(\mathbf{r})$ component, by using the cylindrical symmetry of the skyrmion. **a**, **b**, It is clear that our skyrmion is composed of two coaxial tori. The two pink rings represent the cores of these two tori where $\langle S_z\rangle$ reaches its maximum negative value of −1/2. **c**, **d**, Show the cross-sections of the two tori.

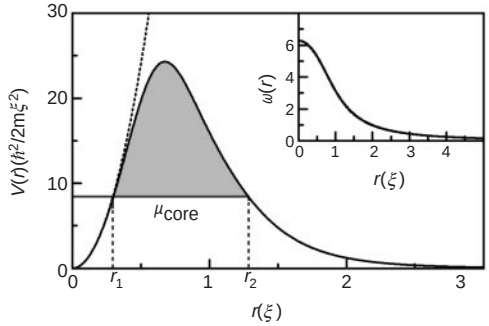

Figure 3 The potential barrier produced by the skyrmion texture. The value of λ used is again approximately ξ which corresponds to 20 core atoms. The lifetime of the skyrmion is determined by the tunnelling of core atoms with a chemical potential μ_{core} to the right of the barrier. The square root of the shaded area is the integrand of equation (4). The dotted curve represents the harmonic approximation to $V(r)$ for small r/λ. The inset shows $\omega(r)$ for the same value of λ.

the centres of the magnetic traps for the two spin species along the z axis[6]. Furthermore, the desired behaviour of the Rabi frequency can be achieved by making, with the first Raman laser, two standing waves in the x and y directions that are both polarized perpendicular to the z axis. For the other Raman laser we only require that it produces a travelling wave with a polarization that has a non-zero projection on the z axis, because we want to realize a $\Delta m = 0$ transition in this case. In the above geometry the skyrmion is created exactly in the plane where the detuning vanishes and in the nodes of the first Raman laser. We note that as the distance between these nodes is generally much bigger than the correlation length, we create in this manner a large skyrmion that will start to shrink but ultimately self-stabilizes at a smaller size. Once created, the skyrmion can be easily observed by the usual expansion experiments that have recently also been used to observe vortices[18]. As with vortex rings, we then observe an almost complete depletion of the condensate in a ring around the position of the skyrmion.□

Methods

To calculate the energy of the skyrmion we solve the equation for the density profile that is obtained from minimizing the energy functional in equation (1). We solve this equation numerically for the region outside the core. Inside the core we solve the equation analytically by using the Thomas–Fermi approximation, which amounts to neglecting the gradients of the density profile. Using our ansatz for $\omega(r)$, the texture gradient potential $V(r) = \hbar^2|\nabla\zeta(\mathbf{r})|^2/2m$ reads:

$$V(r) = \frac{\hbar^2}{2m}\frac{32}{\lambda^2}\frac{(r/\lambda)^2[3 + 2(r/\lambda)^4 + 3(r/\lambda)^8]}{[1 + (r/\lambda)^4]^4} \quad (3)$$

For small r/λ this potential can be approximated by a harmonic potential with a characteristic frequency $\omega_0 = \sqrt{96}\hbar^2/2m^2\lambda^4$ and width $l = \lambda/\sqrt{96}$, as shown in the dotted curve in Fig. 3. Specifically, the use of a Thomas–Fermi approximation is justified when the ratio $2Na/l = 2\sqrt{96}Na/\lambda$ is bigger than 1. From Fig. 1, we observe that this ratio equals approximately 1 for $N = 4$ and increases for larger N.

The lifetime of the skyrmion is estimated by calculating the tunnelling rate from the core to the outer region over the barrier $V(r)$. To this end we employ the following WKB (Wentzel, Kramers and Brillouin) expression for the tunnelling rate[19]:

$$\Gamma = \frac{\omega_0}{2\pi}\exp\left[-2\int_{r_1}^{r_2} dr\sqrt{\frac{2m}{\hbar^2}(V(r) - \mu_{\text{core}})}\right] \quad (4)$$

where μ_{core} is the chemical potential of the core atoms. The radial points r_1 and r_2 are the points where $V(r)$ and μ_{core} intersect, as shown in Fig. 3. The chemical potential μ_{core} is calculated by differentiating the total energy of the core with respect to the number of core atoms.

Received 15 November 2000; accepted 20 April 2001.

1. Myatt, C. J., Burt, E. A., Ghrist, R. W., Cornell, E. A. & Wieman, C. E. Production of two overlapping Bose–Einstein condensates by sympathetic cooling. *Phys. Rev. Lett.* **78,** 586–589 (1997).
2. Stamper-Kurn, D. M. *et al.* Optical confinement of a Bose–Einstein condensate. *Phys. Rev. Lett.* **80,** 2027–2030 (1998).
3. Stenger, J. *et al.* Spin domains in ground-state Bose–Einstein condensates. *Nature* **396,** 345–348 (1998).
4. Hall, D. S., Matthews, M. R., Ensher, J. R., Wieman, C. E. & Cornell, E. A. Dynamics of component separation in a binary mixture of Bose–Einstein condensates. *Phys. Rev. Lett.* **81,** 1539–1542 (1998).
5. Stamper-Kurn, D. M. *et al.* Quantum tunneling across spin domains in a Bose condensate. *Phys. Rev. Lett.* **83,** 661–664 (1999).
6. Matthews, M. R. *et al.* Watching a superfluid untwist itself: Recurrence of Rabi oscillations in a Bose–Einstein condensate. *Phys. Rev. Lett.* **83,** 3358–3361 (1999).
7. Matthews, M. R. *et al.* Vortices in a Bose–Einstein condensate. *Phys. Rev. Lett.* **83,** 2498–2501 (1999).
8. Ho, T.-L. Spinor Bose condensates in optical traps. *Phys. Rev. Lett.* **81,** 742–745 (1998).
9. Ohmi, T. & Machida, K. Bose–Einstein condensation with internal degrees of freedom in alkali atom gases. *J. Phys. Soc. Jpn* **67,** 1822–1825 (1998).
10. Law, C. K., Pu, H. & Bigelow, N. B. Quantum spins mixing in spin Bose–Einstein condensates. *Phys. Rev. Lett.* **81,** 5257–5261 (1998).
11. Ho, T.-L. & Yip, S.-K. Fragmented and single condensate ground states of spin-1 Bose gas. *Phys. Rev. Lett.* **84,** 4031–4034 (2000).
12. Yip, S.-K. Internal vortex structure of a trapped spinor Bose–Einstein condensate. *Phys. Rev. Lett.* **83,** 4677–4681 (1999).
13. Williams, J. E. & Holland, M. J. Preparing topological states of a Bose–Einstein condensate. *Nature* **401,** 568–572 (1999).
14. Skyrme, T. H. R. A non-linear field theory. *Proc. R. Soc. Lond. A* **260,** 127–138 (1961).
15. Skyrme, T. H. R. A unified field theory of mesons and baryons. *Nucl. Phys.* **31,** 556–569 (1962).
16. Julienne, P. S., Mies, F. H., Tiesinga, E. & Williams, C. J. Collisional stability of double Bose condensates. *Phys. Rev. Lett.* **78,** 1880–1883 (1997).
17. Côté, R. *et al.* Collective excitations, NMR, and phase transitions in Skyrme crystals. *Phys. Rev. Lett.* **78,** 4825–4828 (1997).
18. Madison, K. W., Chevy, F., Wohlleben, W. & Dalibard, J. Vortex formation in a stirred Bose–Einstein condensate. *Phys. Rev. Lett.* **84,** 806–809 (2000).
19. Stoof, H. T. C. Macroscopic quantum tunneling of a Bose–Einstein condensate. *J. Stat. Phys.* **87,** 1353–1366 (1997).

Acknowledgements

We thank M. Bijlsma for help in the numerical calculations and for helpful remarks. We also thank J. Anglin, G.'t Hooft, D. Olive and J. Smit for useful discussions. This work is supported by the Stichting voor Fundamenteel Onderzoek der Materie (FOM), which is financially supported by the Nederlandse Organisatie voor Wetenschappelijk Onderzoek (NWO).

Correspondence and requests for materials should be addressed to U.A.K. (e-mail: u.alkhawaja@phys.uu.nl).

Interplay of magnetism and high-T_c superconductivity at individual Ni impurity atoms in $Bi_2Sr_2CaCu_2O_{8+\delta}$

E. W. Hudson*†, K. M. Lang*, V. Madhavan*, S. H. Pan*‡, H. Eisaki§‖, S. Uchida§ & J. C. Davis*

* *Department of Physics, University of California, Berkeley, California 94720, USA*
† *National Institute of Standards and Technology, Gaithersburg, Maryland 20899, USA*
‡ *Department of Physics, Boston University, Boston, Massachusetts 02215, USA*
§ *Department of Superconductivity, University of Tokyo, Yayoi, 2-11-16 Bunkyo-ku, Tokyo 113-8656, Japan*
‖ *Department of Applied Physics, Stanford University, Stanford, California, 94205-4060, USA*

Magnetic interactions and magnetic impurities are destructive to superconductivity in conventional superconductors[1]. By contrast, in some unconventional macroscopic quantum systems (such as superfluid ^{3}He and superconducting UGe_2), the superconductivity (or superfluidity) is actually mediated by magnetic interactions. A magnetic mechanism has also been proposed for high-temperature superconductivity[2–6]. Within this context, the fact that magnetic Ni impurity atoms have a weaker effect on superconductivity than non-magnetic Zn atoms in the high-T_c superconductors has been put forward as evidence supporting a magnetic mechanism[5,6]. Here we use scanning tunnelling microscopy to determine directly the influence of individual Ni atoms on the local electronic structure of $Bi_2Sr_2CaCu_2O_{8+\delta}$. At each Ni site we observe two d-wave impurity states[7,8] of apparently opposite spin polarization, whose existence indicates that Ni retains a magnetic moment in the superconducting state. However, analysis of the impurity-state energies shows that quasiparticle scattering at Ni is predominantly non-magnetic. Furthermore, we show that the superconducting energy gap and correlations are unimpaired at Ni. This is in strong contrast to the effects of non-magnetic Zn impurities, which locally destroy superconductivity[9]. These results are consistent with predictions for impurity atom phenomena[5,6] derived from a magnetic mechanism.

In our studies we use two different $Bi_2Sr_2Ca(Cu_{1-x}Ni_x)_2O_{8+\delta}$ (BSCCO) single crystals, grown by the floating-zone technique. These crystals have $x = 0.005$ with $T_c = 83$ K and $x = 0.002$ with $T_c = 85$ K, respectively. The Ni atoms substitute for Cu atoms in the superconducting CuO_2 plane and are believed to be in the $Ni^{2+}3d^8$ electronic state, as compared to the $Cu^{2+}3d^9$ of Cu. Above the superconducting transition temperature T_c each Ni atom possesses a strong magnetic moment of around $1.5\mu_B$ (ref. 10). The samples